On the impact of model accuracy for active damping of a viscoelastic beam

Hans Norlander

May 11, 2011

Abstract

How much do model errors influence the closed loop performance? This question is investigated for the control problem of designing active damping of vibrations in a viscoelastic cantilever beam. The beam is physically modeled using Fourier transformed Euler-Bernoulli beam equations. For control design the standard LQG technique is employed, and two different finite order models are used. One is based on truncated modal analysis of the system, and the other model is numerically fitted with respect to the frequency response of the physically theoretical model. The so obtained controllers are evaluated on the physical model with respect to disturbance attenuation and robustness for stability. It is found that all controllers stabilizes the system and attenuates the vibrations, but the controllers based on the numerically fitted model perform notably better than those based on truncated modal analysis.

1 Introduction

In automatic control there are two assertions that are often stated as being true, and usually taught to students in introductory control courses already. The first "truth" is that in order to achieve good control you need to have a good model, and that the better the model is, the better performance of the closed loop system can be obtained. The second "truth" is that by the use of feedback a good performance can be obtained although the model used (if any) in the controller design is very crude, *i.e.* feedback has the property of being very "forgiving" with respect to model errors (uncertainties). Although these two statements do not exclude each other — they both are really true in many senses — they do somehow point in opposite directions concerning the requirements on the model.

The purpose of the present study is to test these two assertions for a more demanding control problem. The control objective is to suppress vibrations in a viscoelastic cantilever beam actuated by piezoelectric elements. The physical model of such a beam is a distributed parameter system, *i.e.* it is governed by partial differential equations (PDEs). However, almost all model based controller design techniques are

based on models expressed as ordinary differential equations (ODEs) of finite order. From that perspective PDEs are usually considered as being of infinite order. In order to enable the use of such controller design techniques any PDE model must be approximated by some finite order ODE. In this work two different low order models of the cantilever beam are used for control design, and the corresponding closed loop systems are compared and evaluated. The two models are reflecting the two assertions mentioned above, in the following sense: The first model is made to have its frequency response as close as possible to that of the true system. The second model is obtained with the aid of a rather "simple" (not theoretically, but in practice) but physically motivated approach, with only minor adjustments made to it to match the frequency response of the true system, and thus resulting in a more "rough" model.

The paper is organised as follows. In Section 2 the Euler-Bernoulli beam equation is presented. This equation is a PDE, and in Section 3 it is used to derive the theoretical, physical model of the beam. This theoretical model is then regarded as the true system description, and will be used in comparisons and evaluations of the obtained models and controllers. In Section 4 the two methods for obtaining finite order models of the true system are presented, and the resulting models are compared to the true system description. The two models are then used for controller design in Section 5, where the standard LQG technique is used in a straightforward manner. In Section 6 the different controllers are applied to the true system description, and the corresponding closed loop systems are compared and evaluated with respect to disturbance attenuation and robustness.

2 The Euler-Bernoulli beam

The simplest distributed model for describing bending vibrations in an *elastic* beam is the Euler-Bernoulli beam equation, see *e.g.* [5],

$$\frac{\partial^2}{\partial x^2}\left(EI\frac{\partial^2}{\partial x^2}w(t,x)\right)+\rho A\frac{\partial^2}{\partial t^2}w(t,x)=\varphi(t,x), \tag{1}$$

where $w(t,x)$ is the vertical deflection of the centerline of the beam at time t and in the point x — see Figure 1 below, showing a cantilever beam. Here ρ is the density, and A is the cross-section area of the beam. The product EI represents the bending stiffness (E is the Young's modulus of elasticity and I is the area moment of inertia about the normal of the x-z-plane as in Figure 1), which in general depends on x. In simple cases, like in this study, EI is piece-wise constant (with respect to x), turning the two second order partial derivatives in (1) into one fourth order partial derivative with respect to x. The right hand side of (1), $\varphi(t,x)$ represents the distribution of external forces acting on the beam. Cases in which these forces are distributed pointwise, like the force $f(t)$ in Figure 1, may be handled in different ways. One possibility is to let $\varphi(t,x)$ be a sum of Dirac's delta functions, and this is used in the derivation of the model structure in Section 4.2. Another way is to set $\varphi(t,x)\equiv 0$, and to let the external forces enter the system in terms of boundary and compatibility conditions, which is the approach used in the remaining part of this section and in Section 3.

A simple way of solving (1) is to utilize the Fourier transform (with respect to time), and to solve the resulting *ordinary* differential equation. This also offers a convenient way of taking damping into account.

As described above, the basic form (1) of the Euler-Bernoulli beam equation is valid for an elastic beam, *i.e.* the beam is totally undamped, and this is due to the idealizations and simplifications used in the derivation of (1). However, all real beams are more or less damped, and in a more realistic treatment it is sometimes relevant to take this damping into account, and in particular so if the beam is made of a viscoelastic material. For viscoelastic materials damping may be accounted for by letting the Young's modulus of elasticity be complex-valued and frequency dependent — see *e.g.* [3] or [7] and the references therein. Young's modulus is then referred to as the *complex modulus*.

Introduce the notation $\hat{s}(\omega)$ for the Fourier transform of a generic signal $s(t)$, and let $E(\omega)$ denote the complex modulus. The Fourier transformed version of the Euler-Bernoulli beam equation is then

$$E(\omega)I\frac{d^4}{dx^4}\hat{w}(\omega,x) - \omega^2\rho A\hat{w}(\omega,x) = 0, \tag{2}$$

which is an ordinary differential equation in x. The solution is determined by the characteristic equation

$$E(\omega)I\lambda^4 - \omega^2\rho A = 0, \tag{3}$$

which has the roots

$$\lambda_k = i^{k-1}\left(\omega^2\frac{\rho A}{E(\omega)I}\right)^{\frac{1}{4}}, \quad k = 1,\ldots,4, \tag{4}$$

where $i = \sqrt{-1}$. The solutions are then

$$\hat{w}(\omega,x) = r^T(\omega,x)c(\omega) \tag{5}$$

where $r^T(\omega,x) = \begin{bmatrix} e^{\lambda_1 x} & e^{\lambda_2 x} & e^{\lambda_3 x} & e^{\lambda_4 x}\end{bmatrix}$ and $c(\omega) = \begin{bmatrix}\alpha(\omega) & \beta(\omega) & \gamma(\omega) & \delta(\omega)\end{bmatrix}^T$. Although not spelled out explicitly here it is understood that $\lambda_k = \lambda_k(\omega) \in \mathbb{C}$ for $k = 1,\ldots,4$, *i.e.* they are frequency dependent and complex-valued.

3 The distributed model

The system under consideration in this study is a cantilever beam, *i.e.* the beam is clamped at one end and free at the other end. The beam is depicted in Figure 1. The beam, which has a rectangular cross-section, is made of a viscoelastic material, and it has two piezoelectric elements attached onto it. These are placed at the same x-position but at opposite sides of the beam, and are used as actuators. By putting an electric voltage over them they will tend to expand or contract, and thereby generate a bending moment on the beam. The voltage over the piezoelectric elements (the same over both elements, but with opposite signs) is the input to the system. The beam is also affected by a disturbance force, $f(t)$ in Figure 1, acting in the z-direction at the free end of the beam (at $x = L$).

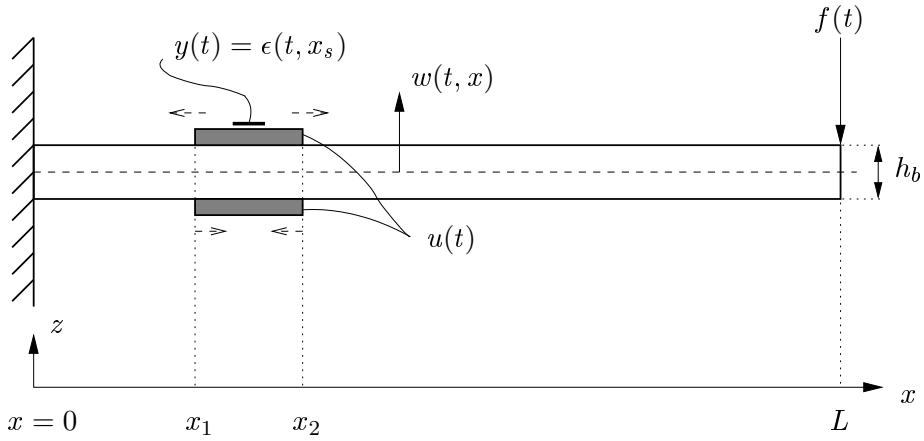

Figure 1: Cantilever beam with piezoelectric elements (shaded). The input u is the voltage over the piezoelectric elements, and the output y is the measured strain, ϵ, at $x_s = \frac{x_1+x_2}{2}$.

Entity	Notation	Value
Beam length [m]	L	0.59
Beam width [m]	b	0.01
Beam thickness [m]	h_b	0.002
Beam density [kg/m^3]	ρ_b	1183
Piezo. length [m]	$x_2 - x_1$	0.0318
Piezo. thickness [m]	h_p	0.00066
Piezo. density [kg/m^3]	ρ_p	7878
Piezo. Young's modulus [N/m^2]	E_p	$5.70 \cdot 10^{10}$
Piezo. position [m]	x_1	0.202
Piezo. charge constant [m/V]	d_{31}	$-2.1 \cdot 10^{-10}$

Table 1: Properties of the beam and the piezoelectric elements.

The system is modeled using the Fourier transformed Euler-Bernoulli equation (2). In order to handle the effect of the piezoelectric elements, the beam is split spatially into three segments along the x-axis, with interfaces in x_1 and x_2 according to Figure 1. Each segment is governed by an equation of type (2). The parameters of the beam are listed in Table 1.

The complex modulus of the viscoelastic material, polymethyl methacrylate (PMMA) is used here, is modeled using a so called generalized standard linear solid model (see [3])

$$E_b(\omega) = \frac{M_R}{2}\left(\frac{1 + i\omega\tau_{\epsilon 1}}{1 + i\omega\tau_{\sigma 1}} + \frac{1 + i\omega\tau_{\epsilon 2}}{1 + i\omega\tau_{\sigma 2}}\right),$$

where $M_R = 4.029 \cdot 10^9$ [N/m^2], and the time constants

$$\tau_{\epsilon 1} = 4.369 \cdot 10^{-3}, \quad \tau_{\sigma 1} = 2.954 \cdot 10^{-3}, \quad \tau_{\epsilon 2} = 450.9 \cdot 10^{-6}, \quad \tau_{\sigma 2} = 365.8 \cdot 10^{-6},$$

all in [s]. These values were experimentally determined in [4].

The system is described by three fourth order ODEs (one for each segment),

$$[E(\omega)I]_k \frac{d^4}{dx^4}\hat{w}_k(\omega,x) - \omega^2 [\rho A]_k \hat{w}_k(\omega,x) = 0 \tag{6}$$

for $k = 1, 2, 3$, so that

$$\begin{aligned} \hat{w}(\omega,x) &= \hat{w}_1(\omega,x) \quad \text{for} \quad 0 < x < x_1, \\ \hat{w}(\omega,x) &= \hat{w}_2(\omega,x) \quad \text{for} \quad x_1 \le x \le x_2 \\ \text{and} \quad \hat{w}(\omega,x) &= \hat{w}_3(\omega,x) \quad \text{for} \quad x_2 < x \le L. \end{aligned}$$

The deflections $\hat{w}_k(\omega,x)$, $k = 1, 2, 3$, are coupled by the boundary conditions

$$\hat{w}_1(\omega,0) = 0, \qquad \frac{d}{dx}\hat{w}_1(\omega,0) = 0, \qquad \hat{M}_3(\omega,L) = 0, \qquad \hat{T}_3(\omega,L) = -\hat{f}(\omega) \tag{7}$$

and the compatibility conditions

$$\begin{aligned} \hat{w}_k(\omega,x_k) &= \hat{w}_{k+1}(\omega,x_k), & \frac{d}{dx}\hat{w}_k(\omega,x_k) &= \frac{d}{dx}\hat{w}_{k+1}(\omega,x_k), \\ \hat{M}_k(\omega,x_k) &= \hat{M}_{k+1}(\omega,x_k), & \hat{T}_k(\omega,x_k) &= \hat{T}_{k+1}(\omega,x_k) \end{aligned} \tag{8}$$

for $k = 1, 2$. Here $\hat{M}_k(\omega,x)$ is the bending moment and $\hat{T}_k(\omega,x)$ is the transversal force. The control input, *i.e.* the voltage $\hat{u}(\omega)$ applied to the piezoelectric elements, enters the system through $\hat{M}_2$, see Appendix A, and the disturbance force $\hat{f}(\omega)$ enters through $\hat{T}_3(\omega,L)$, as seen from (7). Since every $\hat{w}_k(\omega,x)$ is governed by its corresponding ODE (6), with solution in accordance with (5), we have

$$\hat{w}_k(\omega,x) = r_k^T(\omega,x)c_k(\omega), \tag{9}$$

where $r_k^T(\omega,x)$ is determined by the corresponding characteristic equation (3), and $c_k(\omega)$, $k = 1, 2, 3$, are determined jointly from the boundary and compatibility conditions (7) and (8). It turns out that the deflection depends linearly (affine) on the external inputs, the control signal $\hat{u}(\omega)$ and the disturbance force $\hat{f}(\omega)$, *i.e.*

$$\hat{w}(\omega,x) = \hat{H}^u(\omega,x)\hat{u}(\omega) + \hat{H}^f(\omega,x)\hat{f}(\omega). \tag{10}$$

A derivation of (10) is found in Appendix A.

Remark The expression (10) gives the frequency response of the deflection. If one, for some known u and f, would like to compute the time response, $w(t,x)$, it is obtained by using the inverse Fourier transform. However, in this work it is mainly the frequency properties of the system that are of interest, and the inverse Fourier transform is not utilized, but (10) is used as it stands. ■

Remark Explicit expressions for $\hat{H}^u(\omega,x)$ and $\hat{H}^f(\omega,x)$ are not easily obtained, and would be rather involved and complex. Still, explicit expressions for these are really not needed since both are easily computed numerically, which is the technique employed in this work. ■

In this study it is not the deflection w but rather the strain, ϵ, that is measured, by a strain gauge. In contrast to the actuators, *i.e.* the piezoelectric elements, the strain gauge is very small and light and its influence on the beam is considered negligible. Therefore it is neglected in the model.

The strain is related to the deflection according to $\hat{\epsilon}(\omega, x) = -\frac{h(x)}{2}\frac{d^2}{dx^2}\hat{w}(\omega, x)$, where $h(x)$ is the thickness of the beam at position x. In order to have actuators and sensor collocated the strain gauge is placed on top of one of the piezo elements, in the middle of the second segment of the beam, *i.e.* at $x_s = (x_1 + x_2)/2$. The measured strain is thus $y(t) = \epsilon(x_s, t)$, and this is regarded as the output (performance variable) of the system.

From input to output the cantilever beam system is described by

$$\hat{y}(\omega) = \hat{G}^u(\omega)\hat{u}(\omega) + \hat{G}^f(\omega)\hat{f}(\omega), \tag{11}$$

where

$$\hat{G}^u(\omega) = -\frac{h_b + 2h_p}{2} \cdot \frac{d^2}{dx^2}\hat{H}^u(\omega, x_s) \quad \text{and} \quad \hat{G}^f(\omega) = -\frac{h_b + 2h_p}{2} \cdot \frac{d^2}{dx^2}\hat{H}^f(\omega, x_s)$$

(since $h(x_s) = h_b + 2h_p$).

In this study two different ways of finding approximate, low order models for model based control design are used. For this reason the coupled ODEs (6), together with the boundary and compatibility conditions (7) and (8) etc, finally resulting in (11), will be regarded as the *true system* (in the sense of an exact model). This is of course a drastic and non-realistic claim, not the least since the Euler-Bernoulli beam-equation is merely a model itself, based on idealized conditions and simplifications. Nevertheless, it will be regarded as the true system, which will be used as a reference when comparing the approximate low order models and the controllers based on these.

4 Finite order models

Two methods for obtaining low order models will be compared here. Method 1 is a rather ad hoc approach, while Method 2 is based on modal analysis of the Euler-Bernoulli beam-equation (1). The system is very resonant, and as it is of infinite order there are infinitely many resonant modes; see for instance Figure 2. The purpose of feedback control of this beam is to dampen the vibrations due to these resonances, and in particular the vibrations caused by a disturbance force acting on the tip of the beam, at $x = L$ as shown in Figure 1. However, any implementable controller must be of finite order, implying that not all, but only a finite number of the resonances can be dampened out. As is apparent from the Bode plot from f to y, see the right graph in Figure 2, the resonance peaks are decreasing with increasing frequency. Therefore it seems reasonable to try to suppress the first few peaks — that would have the biggest impact. This also indicates that the model used in the control design should have a good fidelity in a frequency range covering at least the resonant modes of interest. In this study the ambition is to suppress the first three resonance peaks.

Due to the resonant nature of the beam both methods used here can be viewed as a sum of second order systems with a small relative damping, where every term represents one resonant mode/peak. Let $G_n^u(s,\theta_j^u)$ and $G_n^f(s,\theta_j^f)$ denote the approximate, finite order models of $\hat{G}^u(\omega)$ and $\hat{G}^f(\omega)$ respectively. The index n indicates the number of modes in the models (*i.e.* the order of the models is $2n$), while θ_j^u and θ_j^f represents the parameter vectors for the model from method $j = 1, 2$. This means that

$$G_n^f(s,\theta_j^f) = \sum_{k=1}^{n} \frac{\psi_{j,k}}{s^2 + 2\zeta_{j,k}\omega_{j,k}s + \omega_{j,k}^2}, \tag{12}$$

where $\psi_{j,k}$, $\omega_{j,k}$ and $\zeta_{j,k}$, $k = 1, \ldots, n$, are the elements of θ_j^f (and likewise for $G_n^u(s,\theta_j)$). (The index j on $\psi_{j,k}$, $\omega_{j,k}$ and $\zeta_{j,k}$ is used here merely to indicate that these differ for the two methods — for brevity they will be omitted in the sequel.)

4.1 Method 1

The idea behind method 1 is to have the frequency response of the model as close as possible to the true system, in the frequency range of interest. In this sense method 1 is equivalent to the "Ad-hoc Approach" presented in [8], where the criterion

$$V(\theta) = \sum_{k=1}^{N} \left| \hat{G}(\omega_k) - G_n(i\omega_k,\theta) \right|^2 W(\omega_k) \tag{13}$$

is (numerically) minimized. Here $W(\omega_k)$ is a frequency-dependent weight. Note that the frequency responses are evaluated at N discrete frequencies. Here $G_n(s,\theta)$ is a rational function with arbitrary but predefined degrees of the numerator and denominator polynomials. However, this direct approach is very sensitive when used for this purpose, *i.e.* for obtaining low-order models of resonant systems — while successfully used to obtain a sixth order model of the beam in [8] (by careful tuning of the weight $W(\omega_k)$) it often fails to produce higher order models. For this reason another ad hoc approach is used here, where the model is obtained in two steps.

Motivated by the proposed structure in (12), the first step is to model each mode

$$\gamma_k(s) = \frac{1}{s^2 + 2\zeta_k\omega_k s + \omega_k^2}, \quad k = 1, \ldots, n, \tag{14}$$

i.e. to determine the natural frequency ω_k and the relative damping ζ_k of each mode. This is easily performed with the criterion (13) in a narrow frequency interval containing the peak corresponding to the mode k (*e.g.* by using the Matlab function *invfreqs*). In this first step no account is made for the order of the sought model — each mode is modeled individually.

With the individual modes available the model can be parameterized as

$$\begin{gathered} G_n(s,\theta) = \sum_{k=1}^{n} \psi_k \gamma_k(s) = \Psi_n^T \Gamma_n(s), \\ \text{where} \quad \Psi_n^T = \begin{bmatrix} \psi_1 & \ldots & \psi_n \end{bmatrix}, \quad \Gamma_n(s) = \begin{bmatrix} \gamma_1(s) & \ldots & \gamma_n(s) \end{bmatrix}^T. \end{gathered} \tag{15}$$

The second step is then to find the linear combination of the modes that is best fitted to the true frequency response, using the criterion (13) and minimizing over Ψ_n. This is a simple linear least squares problem and the solution is readily obtained as the solution to the corresponding normal equation, see *e.g.* [9].

In this work $G_n^f(s, \theta_1^f)$ is modeled exactly as described above, which means that its magnitude will have a roll off of second order for high frequencies. However, as is evident from *e.g.* Figure 2 (upper left graph), $\hat{G}^u(\omega)$ is not strictly proper (but still proper). Due to this a direct (feedthrough) term is added to $G_n^u(s, \theta_1^u)$, which is easily handled by letting $\Psi_n^T = \begin{bmatrix} \psi_0 & \psi_1 & \dots & \psi_n \end{bmatrix}$ and $\Gamma_n(s) = \begin{bmatrix} 1 & \gamma_1(s) & \dots & \gamma_n(s) \end{bmatrix}^T$ in (15) for this case.

4.2 Method 2

Method 2 is used in *e.g.* [6], and is based on modal analysis of the Euler-Bernoulli beam-equation (1) (the elastic case), see *e.g.* [5]. This approach is based on the assumption that the solution to (1) is separable, and can be written as $w(t, x) = \phi(x)q(t)$, which, when put into (1), leads to an eigenvalue problem. As a consequence the solution of (1) can be expressed as the infinite sum

$$w(t, x) = \sum_{k=1}^{\infty} \phi_k(x) q_k(t),$$

where $\phi_k(x)$ are the eigenfunctions for the eigenvalue problem. The shapes of these eigenfunctions depend on the boundary conditions of (1). The eigenfunctions $\phi_k(x)$ are orthogonal, and by exploiting this property the partial differential equation (1) can be transformed into an infinite number of decoupled second order *ordinary* differential equations in $q(t)$,

$$\ddot{q}_k(t) + \omega_k^2 q_k(t) = f_k(t), \quad k = 1, 2, \dots, \tag{16}$$

where ω_k^2, $k = 1, 2, \dots$ are the eigenvalues, and $f_k(t)$ is the inner product of $\varphi(t, x)$ and $\phi_k(x)$. By taking the Laplace transform of (16) , the solution of (1) can finally be written as

$$W(s, x) = \sum_{k=1}^{\infty} \frac{\phi_k(x)}{s^2 + \omega_k^2} F_k(s). \tag{17}$$

(See [5] for a thorough treatment of the method.)

In method 2 a finite order model of the system is simply obtained by truncating the infinite sum (17), *i.e.* keeping the modes of interest and omitting the remaining ones. The advantage is that the resonant modes are expressed explicitly in the sum, but also that the so obtained model is valid for all of the beam — the dependence of the spatial coordinate x remains in the finite order model. This, however, is due to the knowledge of the eigenfunctions, $\phi_k(x)$. Unfortunately, explicit expressions for the eigenfunctions are easily obtained only for very simple conditions of the beam in terms of geometry, homogeneity etc. Also, as indicated above, the modal analysis approach is valid only for the elastic case, where the resonant modes are totally undamped.

In a more realistic case, like the one in this study, the method is not applicable unless the system is approximated with a simpler model (w.r.t. geometry, homogeneity etc) for which the modal analysis is more easily performed. To account for damping the denominators in the individual terms in (17) can be complemented with a damping term, so that the denominators become $s^2 + 2\zeta_k\omega_k s + \omega_k^2$, where ζ_k is the damping ratio for mode k. The damping ratios ζ_k then must be chosen in some appropriate way.

In this particular case the following simplifications are made in order to perform the modal analysis: The beam is assumed to be homogeneous, which means that the effect of the actuators, the piezoelectric elements, is neglected. Hence, A, ρ, E and I are assumed to be constant all over the beam. Also, the damping ratios are all set to the same value, $\zeta_k = \zeta$ for all k. Since it is the strain ϵ that is measured and regarded as output, rather than the deflection w, the system will finally be modeled as

$$Y(s) = G_n^u(s, \theta_2^u)U(s) + G_n^f(s, \theta_2^f)F(s) \tag{18}$$

with

$$\begin{aligned} G_n^u(s, \theta_2^u) &= C_u \sum_{k=1}^{n} \frac{\phi(x_s)\left[\phi_k'(x_2) - \phi_k'(x_1)\right]}{s^2 + 2\zeta\omega_k s + \omega_k^2} \\ \text{and} \quad G_n^f(s, \theta_2^f) &= C_f \sum_{k=1}^{n} \frac{\phi_k''(x_s)\phi_k(L)}{s^2 + 2\zeta\omega_k s + \omega_k^2}, \end{aligned} \tag{19}$$

where $x_s = (x_1 + x_2)/2$ as previously, $\phi'(x)$ and $\phi''(x)$ denotes the first and second derivative of $\phi(x)$ respectively, and C_u and C_f are constants that depend on the geometry and properties of the (simplified) beam — see Appendix B for a derivation.

It should be noted that the natural frequencies ω_k and the constants C_u and C_f are determined by A, ρ, E and I for the *simplified* beam. Since the simplified beam is fictional these properties can be chosen to somehow reflect the corresponding average properties for the actual beam. Here this is exploited to obtain as good fidelity as possible to the true system for low frequencies, including the first resonant mode. More specifically, rather then finding suitable values of A, ρ, E and I explicitly, ω_1 and ζ are chosen to match the first peak in the frequency response with that of the true system, and C_u and C_f are chosen to obtain correct static gains, *i.e.* so that $G_n^u(0, \theta_2^u) = \hat{G}^u(0)$ and $G_n^f(0, \theta_2^f) = \hat{G}^f(0)$. It is stressed that all the natural frequencies depend on A, ρ, E and I, which has the consequence that once ω_1 is chosen, all the other ω_k (for $k = 2, \dots$) are also implicitly determined. Also, while the damping ratio ζ is artificial and hence does not influence other parameters in the model, by setting all damping ratios identical, this choice will have influence on all the resonant modes.

4.3 Comparison of models

In this section models obtained with Methods 1 and 2 are compared with the true system (11). In Figure 2 the Bode plots of models with 11 modes (22:nd order models) are shown together with the Bode plot of the true system. As can be seen the frequency response of the model from method 1 (will be referred to as model

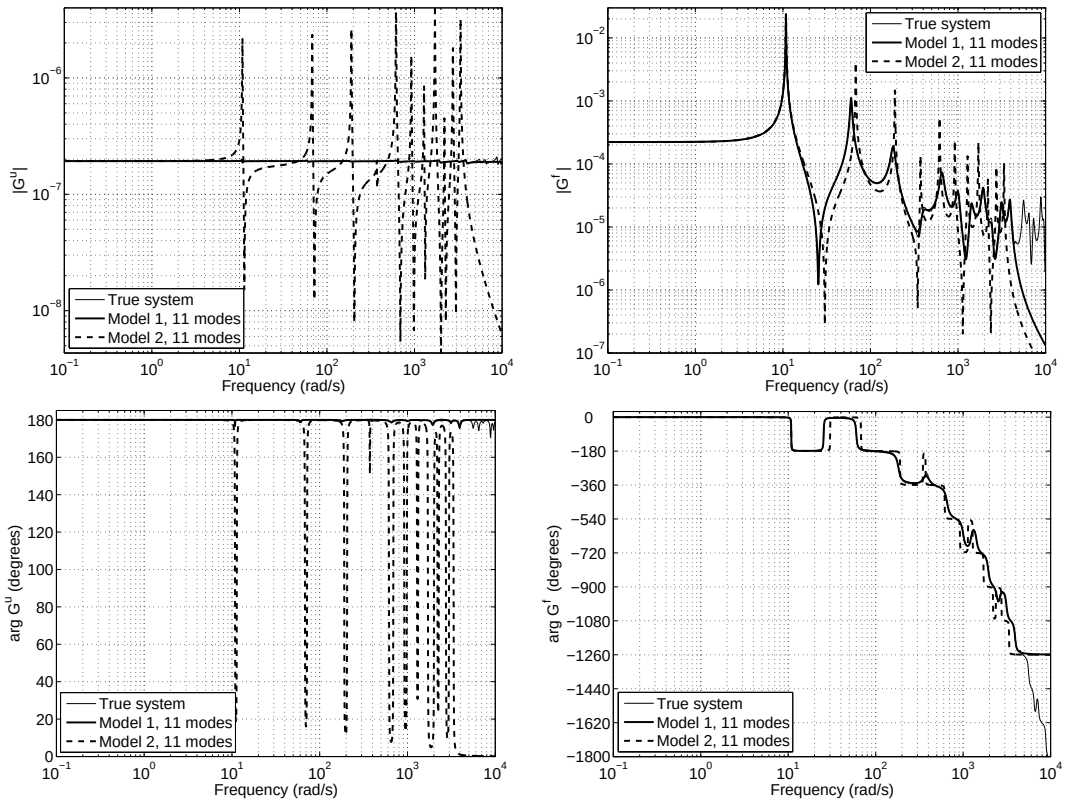

Figure 2: Bode plots of the true system and the models obtained by methods 1 and 2 with 11 modes. Upper and lower graphs shows the magnitude and the phase respectively, the left and right graphs shows the $u-y$- and $f-y$-channels respectively.

1 in the sequel) is very close to that of the true system. In the channel from the disturbance f to the output y this holds for the frequency band up to the eleventh resonance peak. For higher frequencies model 1 has a second order roll off, while the true system continues with resonance peaks. In the channel from the input u to the output y the deviation for higher frequencies is rather small, but this is mainly due to that $\hat{G}^u(\omega)$ is almost constant and that model 1 has a feed through term in that channel.

Since the true system is only known in terms of its frequency response for a finite bandwidth, model 1 with eleven modes will be used for time response simulations of the closed loop systems in Section 6.

The model obtained with method 2 (will be referred to as model 2 in the sequel) differs from the true system to a much larger degree than model 1. In the input-output channel, from u to y, the resonance peaks are significantly higher than for the true system (and for model 1). The reason for this is the manouevre of adjusting C_u for a correct static gain; the omitted modes contributes considerably to the static gain of the infinite order model $G^u_\infty(s, \theta^u_2)$ in (18), so when scaling the static gain the resonance peaks of the included modes are significantly magnified. (This effect is evident when comparing model 2 with eleven modes and with three modes, as shown in Figures 2 and 3 respectively — the peaks for the latter are even higher than for the former due to the eight omitted modes.)

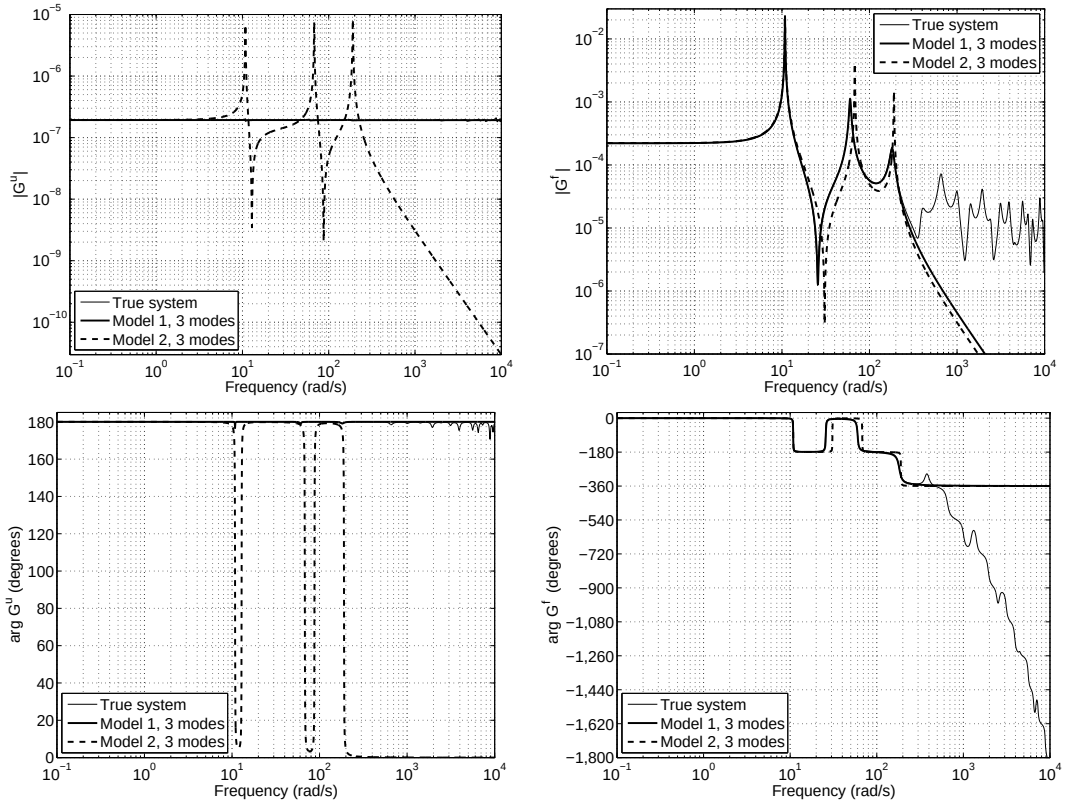

Figure 3: Bode plots of the true system and the models obtained by methods 1 and 2 with 3 modes. Upper and lower graphs shows the magnitude and the phase respectively, the left and right graphs shows the $u-y$- and $f-y$-channels respectively.

In the f-y-channel, from disturbance to output, the frequency response of model 2 is fairly close to the true system, although not nearly as close as model 1 is. Except from the first one the resonance peaks are slightly misplaced compared to the true ones. Nevertheless model 2 captures the general characteristics of the system, in terms of the appearance of peaks and notches. This is an obvious strength of method 2, which makes it rather reliable in this specific sense.

In Figure 3 the frequency responses of models with three modes (sixth order models) are shown. It is these models that will be used in the controller design in Section 6. Once again it is observed that model 1 is very close to the true system up to and including the third resonance peak. Model 2 though differs more from the true system in the considered frequency band. In the u-y-channel the same phenomenon occurs for the same reason as for the 11 mode-models described above. In the f-y-channel the first resonance peak is modeled very well while the second and third ones, as well as the notch at $\omega = 25$ rad/s, are slightly displaced.

5 Controller design

The purpose of this study is to investigate the effect of the model on the performance of the closed loop system. It is the models 1 and 2, as described in Section 4, that are

used for model based control design, and then the corresponding closed loop systems are compared and evaluated. For the controller design the standard linear quadratic Gaussian (LQG) control design technique is employed. More specifically, with the models in state space form as

$$\dot{x}(t) = Ax(t) + Bu(t) + Nf(t), \tag{20}$$
$$y(t) = Cx(t) + Du(t) + e(t), \tag{21}$$

the criterion

$$J = E\left[\int_0^\infty \left(Q_1 y(t)^2 + Q_2 u(t)^2\right) dt\right] \tag{22}$$

is minimized. In the model (20)–(21) $f(t)$ is (as before) the disturbance force, acting at the free end of the beam, and $e(t)$ is the measurement noise. Both these are scalar and are assumed to be random with $E[f(t+\tau)f(t)] = R_1\delta(\tau)$, $E[e(t+\tau)e(t)] = R_2\delta(\tau)$ and $E[f(t+\tau)e(t)] \equiv 0$ (*i.e.* white noise with the intensities R_1 and R_2). The factors $Q_1 \geq 0$ and $Q_2 > 0$ in (22) are weights that can be regarded as design parameters.

The resulting controller is the control law $u(t) = -L\hat{x}(t)$, where $\hat{x}(t)$ is the estimated state vector obtained from the Kalman filter

$$\hat{x}(t) = A\hat{x}(t) + Bu(t) + K(y(t) - C\hat{x}(t) - Du(t)). \tag{23}$$

The feedback gain L (not to be confused with the length of the beam) is a row vector which depends on the ratio Q_1/Q_2, and the Kalman gain K is a column vector which depends on the ratio R_1/R_2. Obviously L and K also depend on the model (20)–(21).

The LQG control design technique will not be further described here; see standard textbooks, *e.g.* [2] and [1], for details of LQG.

The main control objective is to reduce vibrations due to the disturbance force f in the frequency range from 0 to 300 rad/s, or, put in another way, to dampen out the three first resonance peaks. For this purpose, the models with three modes are used in the control design.

When performing analysis and/or control design on a system it is very important to be aware of the sizes of the different signals involved, particularly when comparing signals of different sorts, like u and y in the criterion (22), and f and e in the Kalman filter. This is also very important in a case like the present one, where the different signals differ with several orders of magnitude. A sensible way to handle this is to scale the different signals to be more or less of the same magnitude. It is reasonable and convenient to scale the signals to have a magnitude equal to one (at the most or on average). Here the signals

$$u = D_u u_s, \quad y = D_y y_s, \quad \text{and } f = D_f f_s \tag{24}$$

have been scaled in the control design. That is, the scaled versions, u_s, y_s and f_s have been used in the model (20)–(21), which has been modified accordingly, and then used to compute the feedback gain L and the Kalman gain K. The scaling then must be accounted for again in the controller before implementing it on the real, unscaled system. Note that the measurement noise e is (and must be) scaled with D_y, as it appears together with y in (21). This means that the noise intensities R_1

Case	Q_1	Q_2	R_1	R_2
(a)	1	0.001	1	1
(b)	1	0.001	1	0.1
(c)	1	0.001	1	0.01

Table 2: Design parameters for cases (a)–(c).

and R_2 corresponds to the scaled versions of f and e. Therefore it is natural to set $R_1 = 1$ and to let R_2 represent the relative size of the measurement noise compared to the magnitude of the measured output y.

The control signal is bounded to the range $|u(t)| \leq 250$ [V], and the disturbance force f is assumed to be of size 1 [N]. Considering this it follows from the frequency responses in Figures 2 and 3 that the measured strain y will roughly be of magnitude 10^{-4} [m/m].

Hence the following scalings are used:

$$D_u = 250, \quad D_y = 10^{-4} \quad \text{and } D_f = 1. \tag{25}$$

The controllers computed will depend on the weights Q_1 and Q_2 and the noise intensities R_1 and R_2 (which can be regarded as design parameters), and of course on the model used in the design. Here it is the effect of the *model* that is investigated, so for the two models identical sets of Q_1, Q_2, R_1 and R_2 have been used. The controllers based on model 1 will be referred to as controller 1, and those based on model 2 will be referred to as controller 2. Three different cases were considered, denoted case (a), (b) and (c), with design parameters according to Table 2. In all three cases Q_1, Q_2 and R_1 were fixed. The choice of Q_1 and Q_2 is considered as a reasonable balance between disturbance attenuation and control effort, while R_1 is motivated by the scaling of f as described above. The only parameter that is changed is thus the noise intensity of the measurement noise, R_2. It is considered as a realistic scenario that the measurement noise is of the same magnitude as the measured output y, or slightly less. This motivates these choices of R_2.

The six controllers will be referred to as controller 1a, controller 1b etc.

6 Evaluation of the controllers

6.1 Disturbance attenuation

The six controllers are evaluated using the true system, in the sense that the frequency responses of the corresponding closed loop systems are computed (remember that the frequency response of the true system is known). In particular the responses from the disturbance force f to the strain y is of interest, as it shows how well the disturbance is attenuated by the controllers. This closed loop system can be represented by

$Y(s) = G^f(s)S(s)F(s)$, where

$$S(s) = \frac{1}{1 + C(s)G^u(s)} \tag{26}$$

is the sensitivity function. Here $C(s)$ is the transfer function of the controller, and $G^u(s)$ and $G^f(s)$ are the presumed transfer functions for the cantilever beam. The magnitude plots for $G^f(s)S(s)$ are shown in Figures 4, 6 and 8 for the cases (a), (b) and (c) respectively. The frequency response $\hat{G}^f(\omega)$ is also shown, for comparison.

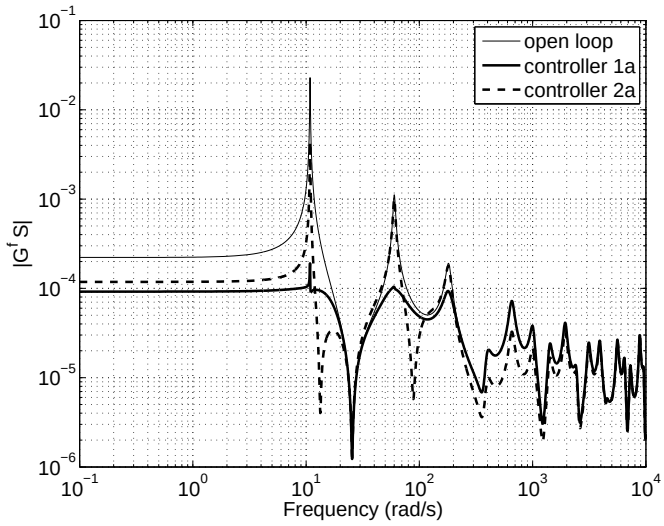

Figure 4: The magnitude of the frequency response from f to y for the open and closed loop systems for case (a), *i.e.* $R_2 = 1$.

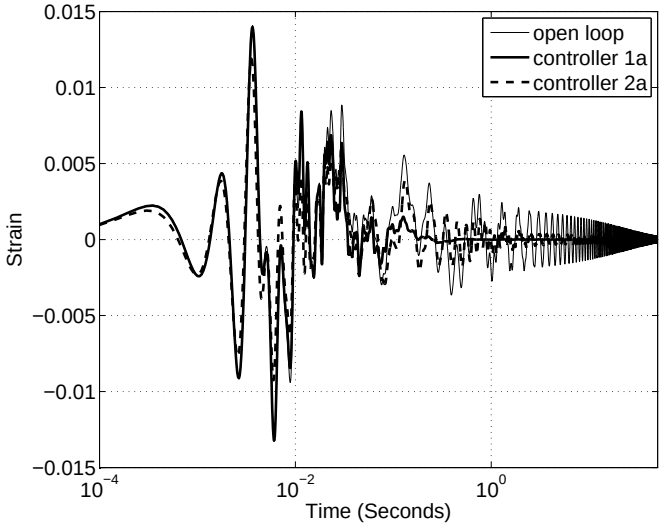

Figure 5: Impulse response for case (a)

Simulations of the impulse responses of $G^f(s)S(s)$ for all six controllers have also been performed. The impulse responses are shown in Figures 5, 7 and 9 for the cases (a), (b) and (c) respectively. The impulse response of $G^f(s)$, *i.e.* the open loop system, is also shown for comparison. Note that the time axes have logarithmic scales in these

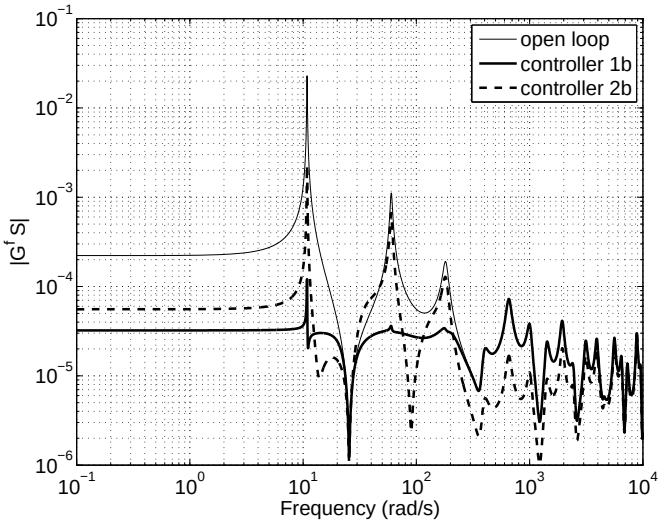

Figure 6: The magnitude of the frequency response from f to y for the open and closed loop systems for case (b), *i.e.* $R_2 = 0.1$.

plots. This rather unorthodox convention is used merely to be able to visualize the behavior in different time scales in one plot only. For these simulations it is though not the true system that has been used, since the true system is known only in terms of its frequency response. Instead model 1 with eleven modes has been used, as it is considered to be very close to the true system in a wide frequency range (see Figure 2).

It could be noticed that all three controllers based on model 2 are unstable. The corresponding closed loop systems are though all stable (judged by the Nyquist criterion, utilizing the frequency response of the true system).

From Figures 4, 6 and 8 it is clear that the controllers 1a–c perform better than the controllers 2a–c *in the intended frequency range*, *i.e.* up to 300 rad/s, including the three first resonant modes. For frequencies higher than 300 rad/s $|G^f(i\omega)S(i\omega)|$ coincides with $|G^f(i\omega)|$ for the controllers 1a–c. It is interesting though that the controllers 2a–c do have disturbance attenuation for frequencies higher than 300 rad/s and thus perform better than the controllers 1a–c in that range, and particularly so in cases (b) and (c).

This is also evident from the impulse response simulations, as shown in Figures 5, 7 and 9. The controllers 1a–c dampen the oscillations within the first few tenths of a second, while the controllers 2a–c need several seconds to dampen the oscillations. This is still a considerable improvement compared to the open loop system, which continues to oscillate for 100 seconds and more. On the other hand, looking at the very first part of the impulse response the controllers 1a–c have no effect until after circa 0.01 seconds, but the controllers 2a–c actually attenuates the oscillations slightly from the start already. This is in line the high frequency attenuation for controller 2 observed in the magnitude plots, as discussed above.

One quantitative measure of the disturbance attenuation achieved with the different controllers is the H_2-norm of $G^f(s)S(s)$. This could be computed in some different

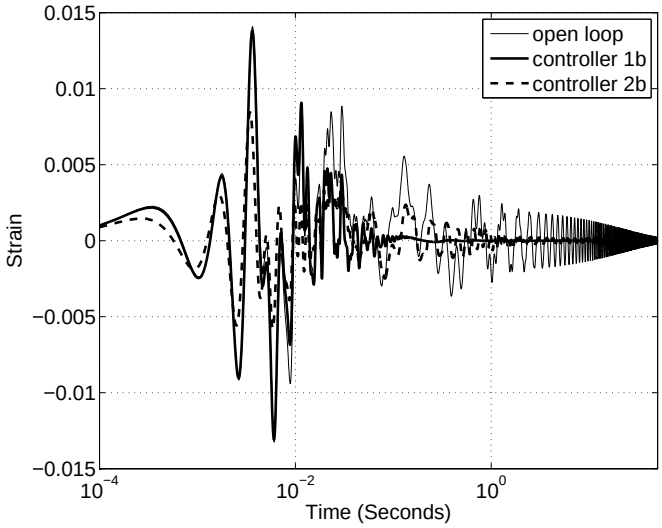

Figure 7: Impulse response for case (b)

Case	Controller 1	Controller 2	Open loop
(a)	$9.3 \cdot 10^{-4}$	$1.7 \cdot 10^{-3}$	$5.2 \cdot 10^{-3}$
(b)	$7.8 \cdot 10^{-4}$	$1.1 \cdot 10^{-3}$	"
(c)	$7.4 \cdot 10^{-4}$	$6.3 \cdot 10^{-4}$	"

Table 3: $||G^f(s)S(s)||_2$ for the controllers in cases (a)–(c).

ways. One way would be to exploit the frequency response of the true system, but this would still only be a truncated approximation, since the frequency response is only known in a finite interval. On the other hand, it might be more relevant to only include lower frequencies. Here though model 1 with eleven modes is used instead for simplicity; the values are then easily computed (using standard software or by solving a Lyapunov equation). The computed values of $||G^f(s)S(s)||_2$ for the different controllers are presented in Table 3. In the cases (a) and (b) controller 1 is the most successful, but in case (c) it is instead controller 2 that has the lowest H_2-norm. The reason for that is the better attenuation for controller 2c in the frequency range above 300 rad/s. Still, it could argued that controller 1c "does the job" better in the intended frequency range (up to 300 rad/s).

6.2 Robustness with respect to stability

Apart from the disturbance attenuation, which is the main control objective, there are also other properties of the closed loop systems that are important, such as stability and robustness with respect to model errors. Particularly in this case, where there are obvious model errors (an infinite order system is approximated with finite order models) the robustness properties are of interest.

A well known result is the following (see *e.g.* [1] or [2]):

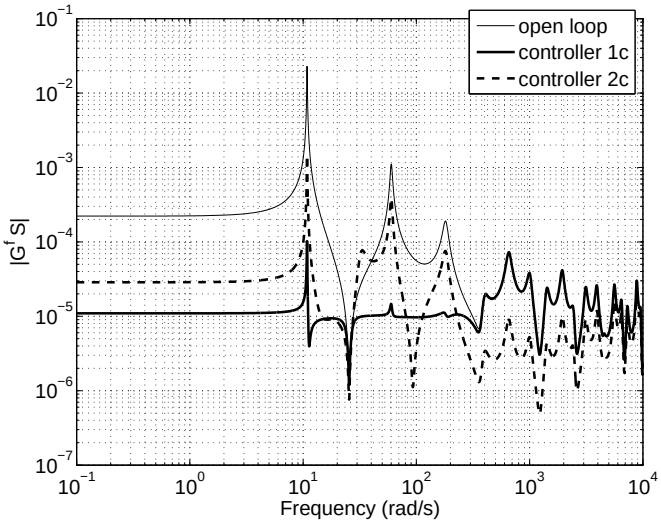

Figure 8: The magnitude of the frequency response from f to y for the open and closed loop systems for case (c), *i.e.* $R_2 = 0.01$.

Theorem 6.1 *A system is modeled as* $Y(s) = G(s)U(s)$. *The true system has the transfer function* $G_0(s) = G(s)(1 + \Delta_G(s))$. *Assume that the control law* $U(s) = -C(s)Y(s)$ *stabilizes the modeled closed loop system*

$$T(s) = \frac{C(s)G(s)}{1 + C(s)G(s)}, \tag{27}$$

and that $||T(s)\Delta_G(s)||_\infty < 1$, *then the true closed loop system is guaranteed to be stable.*

Here $T(s)$ is the complementary sensitivity function, and $\Delta_G(s)$ is the relative model error. Generally $\Delta_G(s)$ is unknown, but with the aid of some (estimated) upper bound $g(\omega)$ (*i.e.* $|\Delta_G(i\omega)| \leq g(\omega)$) the result is still very useful in practice.

In contrast to the normal case the frequency response of the relative model error, $\Delta_G(i\omega)$, is actually known in this particular case. To investigate the robustness properties obtained with the different controllers, $|T(i\omega)\Delta_G(i\omega)|$ is computed for each case — the condition $||T(s)\Delta_G(s)||_\infty < 1$ is equivalent to $|T(i\omega)\Delta_G(i\omega)| < 1$ for all ω. Figure 10 shows $|T(i\omega)\Delta_G(i\omega)|$ when the controllers 1a–c are used (on model 1), and Figure 11 shows it for the case when the controllers 2a–c are used (on model 2). It should be noticed here that the complementary sensitivity function in Theorem 6.1 is computed for the *model* and not for the true system. Figure 10 shows that the robustness condition in Theorem 6.1 is fulfilled with a very good margin for the case where the controllers 1a–c are used. However, when the controllers 2a–c are used the condition is not fulfilled, and as seen in Figure 11 $|T(i\omega)\Delta_G(i\omega)|$ has peaks exceeding 10 for all three controllers. As mentioned above, all the closed loop systems are really stable, and it is stressed that Theorem 6.1 provides a *sufficient* condition for stability — it is not a necessary condition. That the condition is violated to such a large degree when the controllers 2a–c are used is mainly due to the rather large relative model error $\Delta_G(s)$ of model 2, and not to the controllers per se — the complementary sensitivity function $T(s)$ does not differ much from the cases based

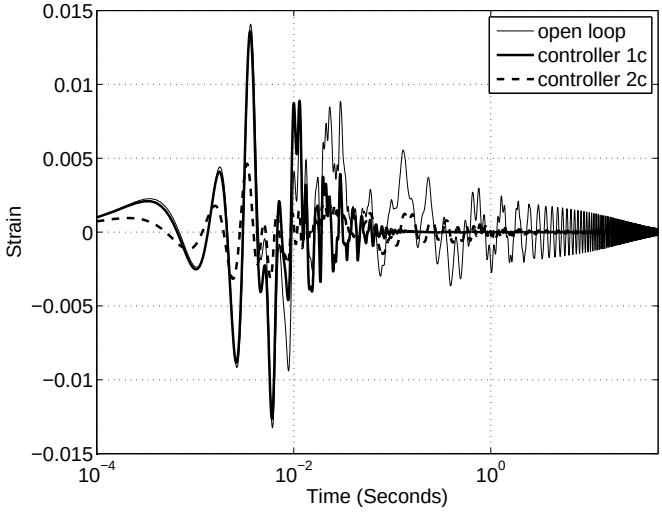

Figure 9: Impulse response for case (c)

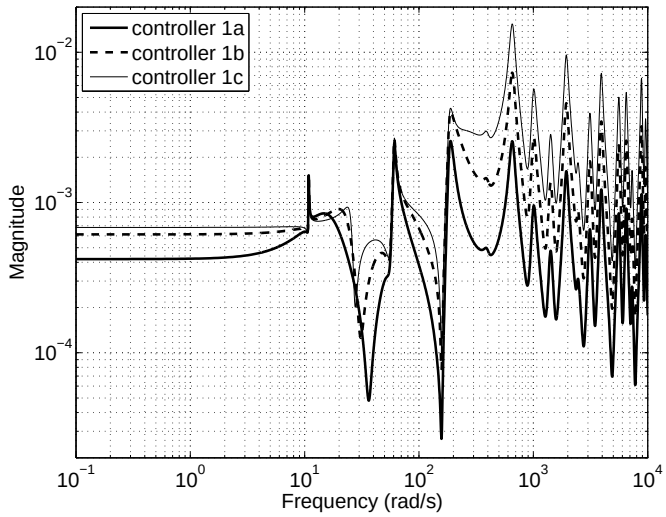

Figure 10: $|T(i\omega)\Delta_G(i\omega)|$ for the controllers 1a–c.

on model 1. The peaks in $|\Delta_G(i\omega)|$ (and thus also on $|T(i\omega)\Delta_G(i\omega)|$) is explained by the exaggeration of the resonance peaks in the u–y-channel in model 2, as discussed in Section 4.3. Since these peaks are much less apparent in the true system, the model errors due to this are less harmful (the opposite situation would probably be much worse).

7 Conclusions

The purpose of the study has been to investigate whether a rather simple but physically motivated model, as obtained from method 2 here, is useful for control design, or if a more elaborated model, as obtained from method 1 here, will give a notably better performance of the closed loop system. This could be rephrased as a test of

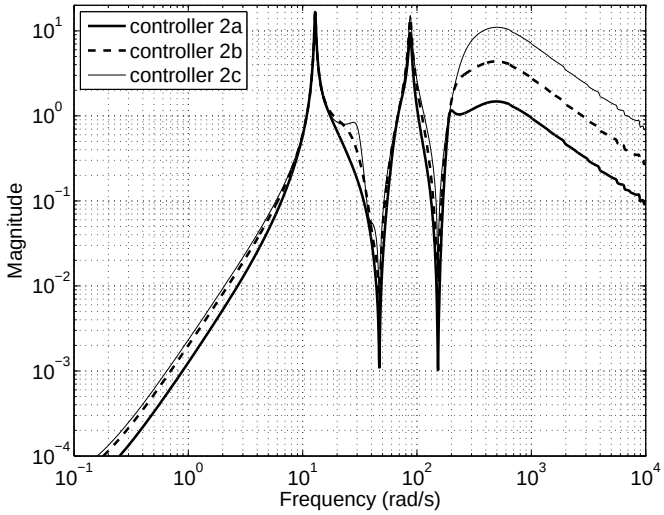

Figure 11: $|T(i\omega)\Delta_G(i\omega)|$ for the controllers 2a–c.

the two assertions mentioned in Section 1, of which the first was "the better the model, the better the control performance", and the second was "good performance is achievable via feedback, also in the presence of imperfect models". Both these statements are found to be more or less true in this particular case, but the first one to a much larger degree than the second one.

The considered system is a viscoelastic beam, actuated by piezoelectric elements and affected by a disturbance force acting on the tip of the beam. The control objective is to attenuate vibrations in the beam due to the disturbance force. Two different finite order models are used for the controller design, and these two models are obtained by using two different approaches, methods 1 and 2. Method 1 is based on numerical fitting of the frequency repsonse (over a finite interval) of the model with respect to that obtained from the Euler-Bernoulli beam equation, which governs the beam. With method 2 the model is simply a truncation of an infinite sum of second order systems obtained from modal analysis of a simplified version of the beam. A set of controllers are designed, based on the two models, and applied to the physical model (the Euler-Bernoulli beam). The corresponding closed loop systems are compared and evaluated with respect to disturbance attenuation and robustness for stability.

To be more precise, the control objective was to attenuate vibrations up to about 300 rad/s, covering the three first resonance peaks, and this is also reflected in the finite order models. When comparing the closed loop performance it is clear that the controllers based on the method 1 model perform considerably better in the intended frequency interval than the controllers based on the method 2 model. It is though interesting to notice that the latter controllers suppress disturbances better than the method 1 controllers for frequencies higher than 300 rad/s. This could be explained by that in method 1 there is a feedthrough term in the model, but not in method 2. Concerning the robustness with respect to stability the method 1 controllers are superior to the method 2 controllers. The main reason for this is that the model error is so much smaller for the method 1 model as compared to the method 2 model.

A Derivation of the distributed model

In this section the Fourier transform of the deflection, $\hat{w}(\omega, x)$ as expressed in (10), is derived. The beam is governed by the Euler-Bernoulli beam equations (6), the boundary conditions (7) and the compatibility conditions (8). The parameters $[E(\omega)I]_k$ and $[\rho A]_k$ in (6) are constant within, but differ between the three segments, $k = 1, 2, 3$. For the first and the third segments they simply are

$$[E(\omega)I]_1 = [E(\omega)I]_3 = E_b(\omega)I_b \quad \text{and} \quad [\rho A]_1 = [\rho A]_3 = \rho_b A_b,$$

where $I_b = \frac{bh_b^3}{12}$ is the area moment of inertia, and $A_b = bh_b$ is cross section area of the beam itself. For the second segment the piezoelectric elements must be taken into account:

$$[E(\omega)I]_2 = E_b(\omega)I_b + 2E_pI_p \quad \text{and} \quad [\rho A]_2 = \rho_b A_b + 2\rho_p A_p,$$

where $I_p = \frac{2b}{3}\left(\left(\frac{h_b}{2} + h_p\right)^3 - \left(\frac{h_b}{2}\right)^3\right)$ and $A_p = bh_p$ are the are moment of inertia and cross section area, respectively, of the piezoelectric elements. The geometric and material parameters are presented in Table 1.

In the first and the third segments the bending moment is

$$\hat{M}_k(\omega, x) = -[E(\omega)I]_k \frac{d^2}{dx^2}\hat{w}_k(\omega, x), \quad k = 1, 3.$$

In the second segment the input voltage $\hat{u}(\omega)$, via the piezoelectric elements, adds an external moment, so that

$$\hat{M}_2(\omega, x) = -[E(\omega)I]_2 \frac{d^2}{dx^2}\hat{w}_k(\omega, x) - C_p\hat{u}(\omega), \tag{28}$$

where $C_p = E_p d_{31} b(h_b + h_p)$, in which d_{31} is the piezoelectric charge constant (also found in Table 1).

The transversal force is

$$\hat{T}_k(\omega, x) = \frac{d}{dx}\hat{M}_k(\omega, x) = -[E(\omega)I]_k \frac{d^3}{dx^3}\hat{w}_k(\omega, x), \quad k = 1, 2, 3.$$

From (9) we have that the deflection is

$$\hat{w}_k(\omega, x) = r_k^T(\omega, x)c_k(\omega), \quad k = 1, 2, 3, \tag{9}$$

where $r_k^T(\omega, x) \in \mathbb{C}^{1\times 4}$ (for fixed ω and x) is governed by the roots of the characteristic equation corresponding to the Euler-Bernoulli beam equation for segment k (compare with (2)–(5)), and $c_k(\omega) \in \mathbb{C}^{4\times 1}$ (for fixed ω) depends on the boundary conditions (7) and the compatibility conditions (8).

For brevity the arguments ω and x are dropped from here on, keeping in mind that $\hat{w}_k$, $\hat{M}_k$, $\hat{T}_k$ and r_k^T depend on both ω and x, while c_k depends on ω only. Thus we have

$$\frac{d\hat{w}_k}{dx} = \frac{dr_k^T}{dx}c_k, \quad \frac{d^2\hat{w}_k}{dx^2} = \frac{d^2r_k^T}{dx^2}c_k, \quad \text{and} \quad \frac{d^3\hat{w}_k}{dx^3} = \frac{d^3r_k^T}{dx^3}c_k.$$

The vectors c_1, c_2 and c_3 contain twelve different elements which together form the unique solution to the linear system of equations constituted by the twelve boundary and compatibility conditions (7) and (8). This system of equations can be solved systematically in the following way: Stack c_1–c_3 into one column vector,

$$c = \begin{bmatrix} c_1 \\ c_2 \\ c_3 \end{bmatrix}.$$

By moving all dependent variables ($\hat{w}_k$, $\hat{M}_k$ and $\hat{T}_k$) to the left side, and the independent variables (the inputs, $\hat{u}$ and $\hat{f}$) to the right side, (7) and (8) can be combined to the linear equation

$$A(\omega)c(\omega) = b_u\hat{u}(\omega) + b_f\hat{f}(\omega),$$

where $A(\omega) \in \mathbb{C}^{12\times 12}$ (for fixed ω) and $b_1, b_2 \in \mathbb{R}^{12\times 1}$ are appropriately chosen. One appropriate choice is

$$A = \begin{bmatrix} r_1^T(0) & \bar{0}_4 & \bar{0}_4 \\ \frac{dr_1^T(0)}{dx} & \bar{0}_4 & \bar{0}_4 \\ r_1^T(x_1) & -r_2^T(x_1) & \bar{0}_4 \\ \frac{dr_1^T(x_1)}{dx} & -\frac{dr_2^T(x_1)}{dx} & \bar{0}_4 \\ -[EI]_1\frac{d^2r_1^T(x_1)}{dx^2} & [EI]_2\frac{d^2r_2^T(x_1)}{dx^2} & \bar{0}_4 \\ -[EI]_1\frac{d^3r_1^T(x_1)}{dx^3} & [EI]_2\frac{d^3r_2^T(x_1)}{dx^3} & \bar{0}_4 \\ \bar{0}_4 & -r_2^T(x_2) & r_3^T(x_2) \\ \bar{0}_4 & -\frac{dr_2^T(x_2)}{dx} & \frac{dr_3^T(x_2)}{dx} \\ \bar{0}_4 & [EI]_2\frac{d^2r_2^T(x_2)}{dx^2} & -[EI]_3\frac{d^2r_3^T(x_2)}{dx^2} \\ \bar{0}_4 & [EI]_2\frac{d^3r_2^T(x_2)}{dx^3} & -[EI]_3\frac{d^3r_3^T(x_2)}{dx^3} \\ \bar{0}_4 & \bar{0}_4 & -[EI]_3\frac{d^2r_3^T(L)}{dx^2} \\ \bar{0}_4 & \bar{0}_4 & -[EI]_3\frac{d^3r_3^T(L)}{dx^3} \end{bmatrix}, \quad b_u = \begin{bmatrix} 0 \\ 0 \\ 0 \\ 0 \\ -C_p \\ 0 \\ 0 \\ 0 \\ -C_p \\ 0 \\ 0 \\ 0 \end{bmatrix}, \quad b_f = \begin{bmatrix} 0 \\ 0 \\ 0 \\ 0 \\ 0 \\ 0 \\ 0 \\ 0 \\ 0 \\ 0 \\ 0 \\ -1 \end{bmatrix},$$

where the arguments on r_k^T indicates the x-position, and $\bar{0}_4 = \begin{bmatrix} 0 & 0 & 0 & 0 \end{bmatrix}$.

Hence

$$c(\omega) = A^{-1}(\omega)b_u\hat{u}(\omega) + A^{-1}(\omega)b_f\hat{f}(\omega),$$

and if we introduce the matrices $P_k \in \mathbb{R}^{4\times 12}$, such that $P_k c = c_k$ for $k = 1, 2, 3$, we finally get

$$\begin{aligned}\hat{w}_k(\omega, x) &= r_k^T(\omega, x)P_kA^{-1}(\omega)b_u\hat{u}(\omega) + r_k^T(\omega, x)P_kA^{-1}(\omega)b_f\hat{f}(\omega) \\ &\triangleq \hat{H}^u(\omega, x)\hat{u}(\omega) + \hat{H}^f(\omega, x)\hat{f}(\omega).\end{aligned}$$

B Modal analysis of the beam

In this section the modal analysis of the cantilever beam, leading to the expressions (17)–(19), will be outlined. The starting point will be the Euler-Bernoulli beam equation as stated in (1). The following simplifying assumption is made: EI and

ρA are real valued and constant along all of the beam. This means that the beam is elastic, and that the piezoelectric elements have no effect on the beam other than adding an external bending moment.

In this approach the external forces (the inputs) are represented by $\varphi(t, x)$ in the right hand side of (1). Since the control input enters the system by generating a bending moment over the beam, it may be less obvious how this appears in (1). For this reason a rough sketch of a derivation of the Euler-Bernoulli beam equation is shown.

Consider a short segment of the beam at position x and of length dx, *i.e.* the segment starts at x and ends at $x+dx$ as shown in Figure 12. It is assumed that the geometry of the segment is fixed, so that there is no deformation. Further it is assumed that the segment is constrained to move in the z-direction (perpendicular to the x-axis — see figure 12), and that it cannot rotate. Finally, $f(t, x)$ represents a distributed external force acting on the beam in the z-direction, which is assumed to be constant over the segment. Let $w(t, x)$ denote the position of the centerline of the segment.

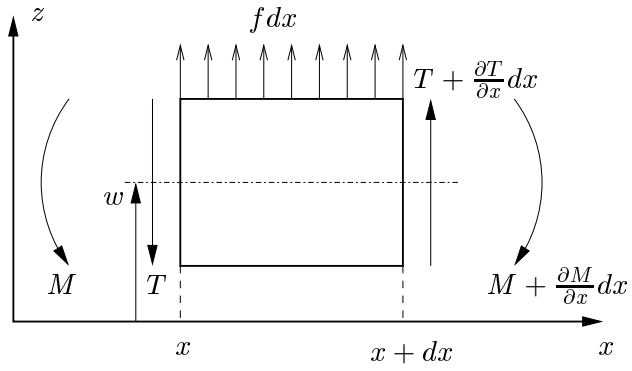

Figure 12: Short beam segment.

Applying Newton's second law to the segment gives

$$-T(t, x) + f(t, x)dx + T(t, x + dx) = \rho A dx \frac{\partial^2 w}{\partial t^2}.$$

Here $T(t, x)$ is the transversal force in the beam, and $f(t, x)dx$ is the total external force on the segment. Using the approximation $T(t, x + dx) \approx T(t, x) + dx\frac{\partial T}{\partial x}$ and dividing with dx then gives

$$f(t, x) + \frac{\partial T}{\partial x} = \rho A \frac{\partial^2 w}{\partial t^2}. \tag{29}$$

Since the segment is not rotating, the net moment about the normal of the x- and z-axes is zero:

$$M(t, x) + T(t, x + dx)dx + f(t, x)dx\frac{dx}{2} - M(t, x + dx) = 0.$$

Here $M(t, x)$ is the total bending moment on the beam. Use the approximations $T(t, x + dx) \approx T(t, x) + dx\frac{\partial T}{\partial x}$, $M(t, x + dx) \approx M(t, x) + dx\frac{\partial M}{\partial x}$, and divide the expression with dx. Furthermore, since dx is considered very small (*i.e.* let $dx \to 0$) higher order terms in dx can be neglected, resulting in

$$T(t, x) = \frac{\partial M}{\partial x}. \tag{30}$$

The total bending moment is $M(t,x) = M_b(t,x) + M_{ext}(t,x)$, where $M_{ext}(t,x)$ is the external bending moment (caused by the piezoelectric elements) and

$$M_b(t,x) = -EI\frac{\partial^2 w}{\partial x^2} \tag{31}$$

is the moment caused by the bending of the beam itself.

Applying (30) and (31) in (29) yields

$$EI\frac{\partial^4 w}{\partial x^4} + \rho A\frac{\partial^2 w}{\partial t^2} = \frac{\partial^2 M_{ext}}{\partial x^2} + f(t,x), \tag{1'}$$

which is the Euler-Bernoulli beam equation (1), but with the effect of the inputs shown explicit.

The modal analysis will now be performed on (1′), with the boundary conditions

$$w(t,0) = 0, \quad \frac{\partial}{\partial x}w(t,0) = 0, \quad \frac{\partial^2}{\partial x^2}w(t,L) = 0, \quad \frac{\partial^3}{\partial x^3}w(t,L) = 0, \tag{32}$$

representing a clamped end at $x = 0$ and a free end at $x = L$ (see Figure 1).

It is assumed that the solution can be expressed as

$$w(t,x) = \sum_{k=1}^{\infty} \phi_k(x) q_k(t), \tag{33}$$

where $\phi_k(x)$, $k = 1, 2, \ldots$, are the eigenfunctions of the eigenvalue problem associated to (1′),

$$\frac{d^4\phi_k}{dx^4} - \lambda_k^4 \phi_k(x) = 0, \tag{34}$$

with boundary conditions

$$\phi_k(0) = 0, \quad \frac{d}{dx}\phi_k(0) = 0, \quad \frac{d^2}{dx^2}\phi_k(L) = 0, \quad \frac{d^3}{dx^3}\phi_k(L) = 0, \tag{35}$$

in analogy with (32). Here λ_k are the eigenvalues corresponding to $\phi_k(x)$, $k = 1, 2, \ldots$. The eigenvalues relate to the natural frequencies of the beam, ω_k, according to

$$\lambda_k^4 = \frac{\rho A}{EI}\omega_k^2.$$

The general solution of (34) is

$$\phi_k(x) = A_k \sin\lambda_k x + B_k \cos\lambda_k x + C_k \sinh\lambda_k x + D_k \cosh\lambda_k x.$$

(Compare with (2) and its solution (5).) Due to the three first boundary conditions in (35) the solution can be written as

$$\phi_k(x) = A_k \left(\sin\lambda_k x - \sinh\lambda_k x - \alpha_k \left(\cos\lambda_k x - \cosh\lambda_k x\right)\right), \tag{36}$$

where

$$\alpha_k = \frac{\sin\lambda_k L + \sinh\lambda_k L}{\cos\lambda_k L + \cosh\lambda_k L}.$$

Furthermore, by using the fourth boundary condition in (35) for the expression (36), the transcendental equation

$$1 + \cos \lambda_k L \cosh \lambda_k L = 0 \tag{37}$$

is obtained, from which the eigenvalues λ_k can be solved for.

The eigenfunctions have the following orthogonality properties [5]:

$$\rho A \int_0^L \phi_k(x)\phi_l(x)dx = \delta_{kl}, \tag{38}$$

$$EI \int_0^L \phi_k(x)\frac{d^4\phi_l}{dx^4}dx = \omega_k^2\delta_{kl}, \tag{39}$$

where δ_{kl} is the Kronecker delta function.

These orthogonality properties are exploited by multiplying $(1')$ with $\phi_k(x)$, and then integrating over x on the interval $0 \leq x \leq L$, resulting in

$$\ddot{q}_k(t) + \omega_k^2 q_k(t) = \int_0^L \phi_k(x)\frac{\partial^2 M_{ext}}{\partial x^2}dx + \int_0^L \phi_k(x)f(t,x)dx, \quad k = 1, 2, \ldots. \tag{40}$$

As before the right member of (40) represents the inputs. The control input enters the system as the bending moment caused by the piezoelectric elements which, in accordance with (28), can be expressed as

$$M_{ext}(t,x) = -C_p u(t)\left(\Theta(x - x_1) - \Theta(x - x_2)\right), \tag{41}$$

where $\Theta(x)$ is Heaviside's step function (*i.e.* the moment only acts where the piezoelectric elements are located). The disturbance force acting at $x = L$ (see Figure 1) can be expressed as

$$f(t,x) = -f(t)\delta(x - L), \tag{42}$$

and here $\delta(x)$ is Dirac's delta function. (The negative sign is due to the downward direction of the force.) Thus, the second term in the right hand side of (40) becomes

$$-f(t)\int_0^L \phi_k(x)\delta(x - L)dx = -\phi_k(L)f(t). \tag{43}$$

Using (41) and the properties

$$\frac{d\Theta}{dx} = \delta(x) \quad \text{and} \quad \int_a^c g(x)\frac{d}{dx}\left[\delta(x - b)\right]dx = -\frac{d}{dx}g(b)$$

for any $a < b < c$ and any continuous function $g(x)$, the first term in the right hand side of (40) turns into

$$-C_p u(t)\int_0^L \left[\phi_k(x)(\delta'(x - x_1) - \delta'(x - x_2))\right]dx = -C_p[\phi_k'(x_2) - \phi_k'(x_1)]u(t). \tag{44}$$

Applying the Laplace transform on (33) and (40) then yields

$$W(s,x) = -C_p\sum_{k=1}^{\infty}\frac{\phi_k(x)[\phi_k'(x_2) - \phi_k'(x_1)]}{s^2 + \omega_k^2}U(s) - \sum_{k=1}^{\infty}\frac{\phi_k(x)\phi_k(L)}{s^2 + \omega_k^2}F(s).$$

Finally, since it is the strain $\epsilon(t, x_s)$ that is regarded as the system output $y(t)$, and since $\epsilon(t, x) = -\frac{h(x)}{2}\frac{\partial^2 w}{\partial x^2}$, the modal analysis ends up in (*cf.* (18)–(19))

$$Y(s) = C_p \frac{h_b + 2h_p}{2} \sum_{k=1}^{\infty} \frac{\phi_k''(x_s)[\phi_k'(x_2) - \phi_k'(x_1)]}{s^2 + \omega_k^2} U(s) + \frac{h_b + 2h_p}{2} \sum_{k=1}^{\infty} \frac{\phi_k''(x_s)\phi_k(L)}{s^2 + \omega_k^2} F(s).$$

References

[1] T. Glad and L. Ljung. *Reglerteori*. Studentlitteratur, 1997.

[2] G. C. Goodwin, S. F. Graebe, and M. E. Salgado. *Control System Design*. Prentice-Hall, Inc., 2001.

[3] L. Hillström. *Estimation of state and identification of complex modulus based on measurements on a bar traversed by waves*. PhD thesis, Department of Materials Science, Uppsala University, 2001.

[4] L. Hillström, U. Valdek, and B. Lundberg. Estimation of the state vector and identification of the complex modulus of a beam. *Journal of Sound and Vibration*, 261:653–673, 2003.

[5] L. Meirovitch. *Principles and Techniques of Vibration*. Prentice-Hall, Inc., 1997.

[6] S. O. R. Moheimani, D. Halim, and A. J. Fleming. *Spatial Control of Vibration: Theory and Experiments*. World Scientific Publishing Co. Pte. Ltd., 2003.

[7] M. Mossberg. *Identification of viscoelastic materials and continuous-time stochastic systems*. PhD thesis, Department of Information Technology, Uppsala University, 2000.

[8] P. Nauclér, H. Norlander, A. Jansson, and T. Söderström. Modeling and control of a viscoelastic piezolaminated beam. In *Proceedings of the 16th IFAC World Congress*, Prague, Czech Republic, July 2005.

[9] T. Söderström and P. Stoica. *System Identification*. Prentice–Hall International, 1989.